Numerical Simulation of Quantum Waveguides

Anton Arnold[1], Matthias Ehrhardt[2] and Maike Schulte[3]

[1] Institut für Analysis und Scientific Computing, TU Wien, Wiedner Hauptstr. 8, 1040 Wien, Austria
[2] Weierstraß–Institut für Angewandte Analysis und Stochastik, Mohrenstr. 39, 10117 Berlin, Germany
[3] Institut für Numerische und Angewandte Mathematik, Universität Münster, Einsteinstr. 62, 48149 Münster, Germany

Abstract. This chapter is a review of the research of the authors from the last decade and focuses on the mathematical analysis of the Schrödinger model for nano–scale semiconductor devices. We discuss *transparent boundary conditions* (TBCs) for the time–dependent Schrödinger equation on a two dimensional domain.

First we derive the two dimensional discrete TBCs in conjunction with a conservative Crank–Nicolson–type finite difference scheme and a compact nine–point scheme. For this difference equations we derive *discrete transparent boundary conditions* (DTBCs) in order to get highly accurate solutions for open boundary problems. The presented discrete boundary–valued problem is unconditionally stable and completely reflection–free at the boundary.

Then, since the DTBCs for the Schrödinger equation include a convolution w.r.t. time with a weakly decaying kernel, we construct *approximate* DTBCs with a kernel having the form of a finite sum of exponentials, which can be efficiently evaluated by recursion.

In several numerical tests we illustrate the perfect absorption of outgoing waves independent of their impact angle at the boundary, the stability, and efficiency of the proposed method. Finally, we apply inhomogeneous DTBCs to the transient simulation of quantum waveguides with a prescribed electron inflow.

1 Introduction

Today's semiconductor devices like transistors and nanoscale split-gate devices are rapidly shrinking in their size. In this context, modeling and numerical simulations play an important role in the development and design of new devices. We focus on devices with ballistic electron transport, such as electron quantum waveguide devices. Their functionality depends on the formation of a 2D electron gas and on wave interference effects (cf. [23]).

Speaking of ballistic transport means that electrons are assumed to not suffer any collision during their transit through the device (e.g. high–purity materials, very small time or length scales, and at low temperatures). A schematic view of such a device, a *double gate metal oxide semiconductor field–effect transistor* (DG–MOS), is shown in Figure 1(a). At the gates there is an applied external potential and the electron transport takes place from source to drain.

We consider the *effective mass approximation*, where the mass m_* is assumed to be constant in homogenized parts of the device. The different materials (e.g. Si, SiO_2) have

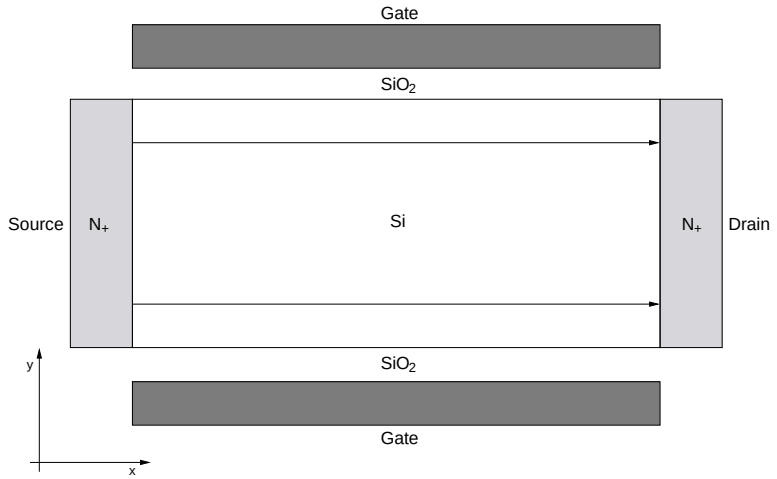

(a) Schematic view of a double gate metal oxide semiconductor field-effect transistor (DG-MOS). The electron transport takes place from source to drain in x-direction. An external potential is applied at the gates.

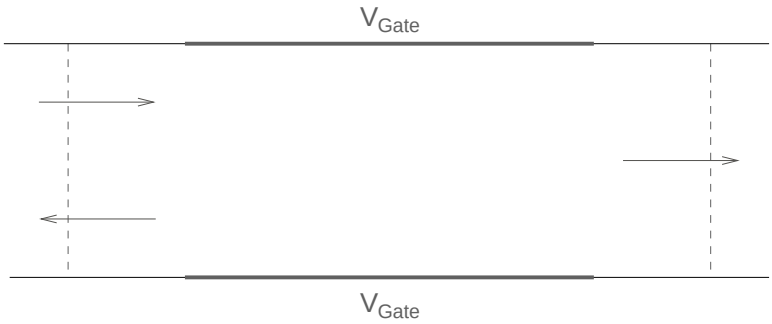

(b) Simplified model of a DG-MOS

Figure 1: Schematic view and simplified model of a DG-MOS.

different effective masses. We simplify this model like it is presented in Figure 1(b), where only one effective mass is used and external potentials V_{Gate} could be applied at the gates. But regarding different materials and therefore different effective masses won't change our proposed model in principle.

Quantum waveguides are novel electronic switches of nanoscale dimensions. They are made of several different semiconductor materials such that the electron flow is confined to small channels or waveguides. Due to their sandwiched structure the relevant geometry for the electron current is roughly two dimensional.

Using external electrostatic potentials the "allowed region" for the electrons, and hence the geometry can be modified. This fact allows to control the current flow through such an electronic device. It makes it a switch, which resembles a transistor, but on a nanoscale (cf. §2.1 of [2], e.g.).

Being quantum particles, the electron transport through a quantum waveguide can be modeled in good approximation by the following two dimensional, *transient Schrödinger equation*

$$\begin{aligned} i\hbar\frac{\partial}{\partial t}\psi(\mathbf{x},t) &= -\frac{\hbar^2}{2m^*}\Delta_{\mathbf{x}}\psi(\mathbf{x},t) + V(\mathbf{x},t)\psi(\mathbf{x},t), \\ &\qquad \mathbf{x}=(x,y)\in\Omega(t),\ t>0, \\ \psi(\mathbf{x},0) &= \psi^I(\mathbf{x}), \quad \mathbf{x}\in\Omega(0), \\ \psi(\mathbf{x},t) &= 0, \quad \mathbf{x}\in\partial\Omega(t), \end{aligned} \tag{1}$$

on a time–dependent geometry $\Omega(t)\subset\mathbb{R}^2$ with initial data $\psi^I\in L^2(\Omega(0))$ and homogeneous Dirichlet boundary conditions. Here, $\hbar$ and m^* denote the Planck constant and effective mass, respectively. The external real valued potential satisfies $V(.,t)\in L^\infty(\Omega(t))$ and $V(\mathbf{x},.)$ is piecewise continuous. The solution ψ to (1) is a time–dependent complex valued wave function with $\psi(.,t)\in L^2(\Omega(t))$.

The spatial domain consists of (very long) leads and the active switching region, which sometimes has the shape of a stub. The structure can be realized as an etched layer $\Omega(t)$ of GaAs between two layers of doped AlGaAs. Here, we shall only consider domains $\Omega(t)$ that are piecewise constant in t and monotonously growing in time. At the jump discontinuities of the domain we shall extent the solution ψ by zero, as a new initialization.

In typical applications, electrons are continuously fed into the leads. Depending on the size and shape of the stub, the electron current is either reflected (*off–state* of the device) or it can pass through the device (*on–state*). Since the applied external potential can modify the stub size, it hence allows to switch the device. Important device data for practitioners are the ratio between the on- and the (residual) off–current as well as the switching time between these two stationary states. These data can be obtained from numerical simulations of the described Schrödinger equation model (1).

The leads are very long compared to the typical size of the active region and they usually only carry (linear combinations of) plane wave solutions. For the efficiency of numerical simulations it is therefore desirable to restrict the simulation model to a small computational region $\tilde{\Omega}(t)$ close to the stub (see Fig. 2). Hence, the leads should be cut off by using artificial boundary conditions. This is possible without changing the solution of the Schrödinger equation by introducing *open boundary conditions* [24], which are non–local in time (convolution type) and in space. Open boundary conditions are called *transparent*, if they yield identical solutions both on the original large domain $\Omega(t)$ and the reduced (computational) domain $\tilde{\Omega}(t)$.

This chapter is organized as follows: In Section 2 we introduce the concept of transparent boundary conditions (TBCs). In Section 3 we derive and analyze a discrete analogue of the analytic TBCs in conjunction with a fourth order compact finite difference scheme of the Schrödinger equation. We present some numerical simulations to illustrate the effectiveness and accuracy of our DTBCs in Section 4. Finally, we give an application of inhomogeneous DTBCs to a 2D waveguide simulation with a T-shaped quantum transistor.

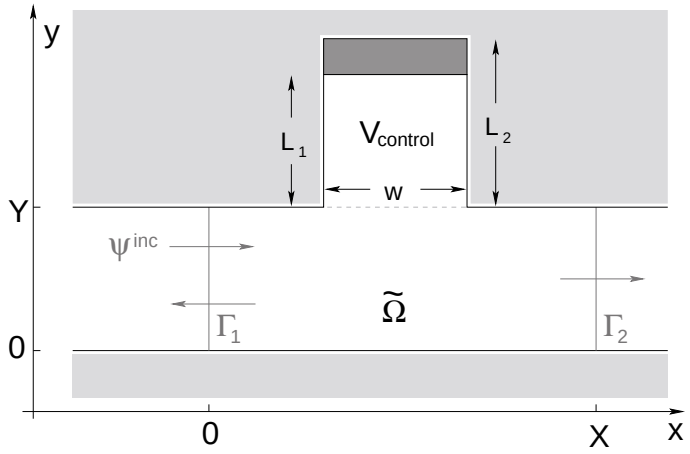

Figure 2: T-shaped structure Ω with the length X, a channel width Y, and a stub width w. It is possible to enlarge the stub length from L_1 to L_2. Inhomogeneous TBCs have to be proposed at $x = 0$, homogeneous TBCs at $x = X$. The inflow at $x = 0$ is modeled by an incoming function $\psi^{\rm inc}$ given by linear combination of plane waves.

2 Transparent boundary conditions for the two dimensional Schrödinger equation

To illustrate the idea of deriving transparent boundary conditions (TBCs) we first consider the one dimensional, time–dependent Schrödinger equation (1) with a potential that satisfies for simplicity the following assumptions: $V(x,t) \equiv V_l$ for $x \le 0$ and $V(x,t) \equiv V_r$ for $x \ge X$ and all $t \ge 0$. For the treatment of nonconstant exterior potentials we refer the reader to [18], [20], [22].

The first step of the derivation is to cut the original *whole–space problem* into three subproblems, the interior problem on the bounded domain $0 < x < X$, and a left and right exterior problem. These problems are coupled by the assumption that the wave function ψ and its spatial derivative ψ_x are continuous across the artificial boundaries at $x = 0$, $x = X$. Hence, the *interior problem* reads

$$\begin{aligned} i\hbar\psi_t &= -\frac{\hbar^2}{2m^*}\psi_{xx} + V(x,t)\psi, \qquad 0 < x < X, \quad t > 0, \\ \psi(x,0) &= \psi^I(x), \quad 0 < x < X, \\ \psi_x(0,t) &= (T_l\psi)(0,t), \quad t > 0, \\ \psi_x(X,t) &= (T_r\psi)(X,t), \quad t > 0. \end{aligned} \tag{2}$$

$T_{l,r}$ denote the *Dirichlet–to–Neumann (DtN) maps* at the left/right boundaries, and they are

obtained by solving the two *exterior problems*:

$$\begin{aligned} i\hbar v_t &= -\frac{\hbar^2}{2m^*} v_{xx} + V_r v, \quad x > X,\ t > 0, \\ v(x,0) &= 0, \quad x > X, \\ v(\infty,t) &= 0 \quad \text{and} \quad v(X,t) = \Phi(t), \quad t > 0,\ \Phi(0) = 0, \end{aligned} \tag{3}$$

which yields $(T_r\Phi)(t) = v_x(X,t)$ and analogously for the left mapping T_l at $x = 0$. Since the potential is constant in the exterior problems, we can solve them explicitly by the Laplace method and thus obtain the two boundary operators $T_{l,r}$ needed in (2) (cf. Fig. 3).

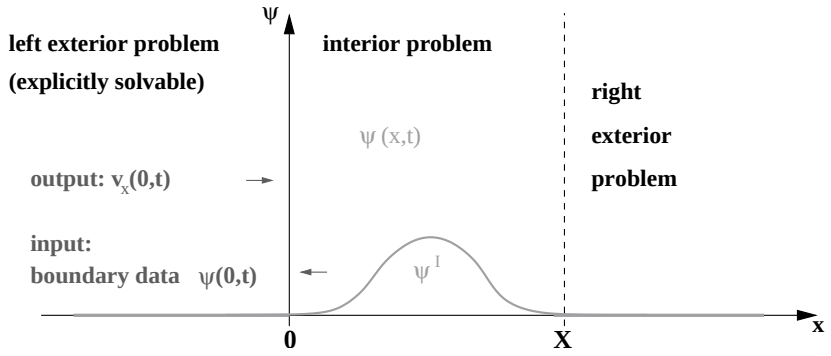

Figure 3: Construction idea for transparent boundary conditions in 1D.

The Laplace transformation of v is given by

$$\hat{v}(x,s) = \int_0^\infty v(x,t)\, e^{-st}\, dt, \quad s = \eta + i\xi,\ \xi \in \mathbb{R},\ \eta > 0 \text{ fixed.}$$

Now the right exterior problem (3) is transformed to

$$\begin{aligned} &\hat{v}_{xx} + i\frac{2m^*}{\hbar}\Big(s + i\frac{V_r}{\hbar}\Big)\hat{v} = 0, \quad x > X, \\ &\hat{v}(X,s) = \hat{\Phi}(s). \end{aligned} \tag{4}$$

Since its solutions have to decrease as $x \to \infty$ (since we have $\psi(.,t) \in L^2(\mathbb{R})$), we obtain

$$\hat{v}(x,s) = e^{-\sqrt[+]{-i\frac{2m^*}{\hbar}(s+i\frac{V_r}{\hbar})}(x-X)}\, \hat{\Phi}(s).$$

Hence, the Laplace–transformed Dirichlet–to–Neumann operator T_r reads

$$\widehat{T_r\Phi}(s) = \hat{v}_x(X,s) = -\sqrt{\frac{2m^*}{\hbar}}\, e^{-i\frac{\pi}{4}}\, \sqrt[+]{s + i\frac{V_r}{\hbar}}\, \hat{\Phi}(s), \tag{5}$$

and T_l is calculated analogously. Here, $\sqrt[+]{\ }$ denotes the branch of the square root with nonnegative real part.

An inverse Laplace transformation of (5) yields the *right TBC* at $x = X$:

$$\psi_x(X,t) = -\sqrt{\frac{2m^*}{\hbar\pi}}\, e^{-i\frac{\pi}{4}} e^{-i\frac{V_r}{\hbar}t} \frac{d}{dt} \int_0^t \frac{\psi(X,\tau)\, e^{i\frac{V_r}{\hbar}\tau}}{\sqrt{t-\tau}}\, d\tau \tag{6}$$

and analogously for the left artificial boundary at $x = 0$. These BCs are *non–local in* t and of memory–type, thus requiring the storage of all previous time levels at the boundary in a numerical discretization. A second difficulty in numerically implementing the continuous TBC (6) is the discretization of the singular convolution kernel. A simple calculation shows that (6) is equivalent to the *impedance boundary condition*:

$$\psi(X,t) = -\sqrt{\frac{\hbar}{2m^*\pi}}\, e^{i\frac{\pi}{4}} \int_0^t \frac{\psi_x(X,t-\tau)\, e^{-i\frac{V_r}{\hbar}\tau}}{\sqrt{\tau}}\, d\tau. \tag{7}$$

Integrating by parts in (6) and carrying out the t-derivative, one sees that the resulting kernel behaves like $\mathcal{O}(t^{-3/2})$ for $t \to \infty$. We remark that the TBC (7) was first derived in 1982 by Papadakis [31] in the context of underwater acoustics. Since the Schrödinger equation (2) has (formally) a similar structure as the heat equation, analogous DtN maps for the heat equation were already given by Carslaw and Jaeger [14] in 1959.

It is possible to extend the one dimensional TBCs (6) to rectangular geometries $(0,X)\times(0,Y)$ in 2D (cf. [8] for details). Now we consider the two dimensional time–dependent Schrödinger equation (1) on the infinite stripe $\Omega = \mathbb{R}\times(0,Y)$. The derivation of two dimensional TBCs is based on taking the partial Fourier series of ψ w.r.t. y:

$$\psi(x,y,t) = \sum_{m\in\mathbb{N}} \hat{\psi}_m(x,t) \sin\left(\frac{m\pi y}{Y}\right). \tag{8}$$

Again we assume that the potential V is constant in each of the two exterior domains: $V(x,y,t) = V_{\text{ext}}$ for $(x,y) \in \Omega\backslash\tilde{\Omega}, t \geq 0$. The time evolution of the modes $\hat{\psi}_m(x,t),\ m \in \mathbb{N}$ is decoupled there. Hence, each mode satisfies at $x = 0$ and $x = X$ a one dimensional TBC

$$\frac{\partial}{\partial\eta}\hat{\psi}_m(x,t) = -\sqrt{2}e^{-i\pi/4}e^{-iV_m t}\sqrt{\partial_t}\left(e^{iV_m t}\hat{\psi}_m(x,t)\right), \quad m\in\mathbb{N}, \tag{9}$$

with the potentials $V_m := V_{\text{ext}} + \frac{1}{2}\left(\frac{m\pi}{Y}\right)^2$, and the unit outward normal vector η. Here, $\sqrt{\partial_t}$ denotes the fractional time derivative of order $1/2$ with the Fourier symbol $\sqrt{-i\omega}$.

Remark 2.1 *Note that the exterior potential V_{ext} in 2D may depend on y. Then, the orthogonal mode decomposition of* (8) *has to use the eigenfunctions of the stationary Schrödinger equation in y with* non–constant *potential $V(y)$ (cf. [12]).*

3 Discrete transparent boundary conditions for the two dimensional Schrödinger equation

The numerical discretizations of the artificial boundary conditions (6), (7) and (9) is delicate, as it may easily render the initial–boundary value problem only conditionally stable

(e.g. [28]). DTBCs for a Crank-Nicolson finite difference discretization of the Schrödinger equation were first given in [6], [17] and [16] (cf. also [4] for a recent review of the various alternative approaches and [32], [33] for enhancements of the discrete TBCs for the Schrödinger equation). In this section we shall follow the "philosophy" of [6], [7], [17], [20] and *derive DTBCs*, instead of *discretizing the continuous TBC* (9).

For the derivation of the DTBCs we will now mimic the derivation of the continuous TBCs presented in Section 2 on a discrete level. First, we will use the unconditionally stable Crank–Nicolson time–discretization scheme combined with a compact nine–point discretization in space. The DTBCs will be constructed directly for the resulting difference equations.

3.1 The difference equations

We first consider the scaled time–dependent Schrödinger equation (TDSE)

$$\begin{aligned} i\frac{\partial}{\partial t}\psi(x,y,t) &= -\frac{1}{2}\Delta\psi(x,y,t) + V(x,y,t)\psi(x,y,t), \quad (x,y)\in\mathbb{R}^2,\, t>0, \\ \psi(x,y,0) &= \psi^I(x,y), \qquad (x,y)\in\mathbb{R}^2, \end{aligned} \tag{10}$$

on the whole space $\mathbb{R}^2$. For the derivation of the associated difference equations we introduce the equidistant grid $\Omega_{\Delta x,\Delta y}$ with the spatial grid points $x_j = j\Delta x$ and $y_k = k\Delta y$ for $j,\, k \in \mathbb{Z}$. We use the uniform time discretization $t_n = n\Delta t$, $n \in \mathbb{N}_0$. Hence, $\psi_{j,k}^n \sim \psi(x_j, y_k, t_n)$ denotes an approximation of the solution $\psi(x,y,t)$ of the Schrödinger equation (10) on the space–time–grid. Using the compact nine–point finite difference scheme in space combined with a Crank-Nicolson time–stepping, the discretized two dimensional scaled Schrödinger equation reads

$$\widetilde{D}^2\,\psi_{j,k}^{n+\frac{1}{2}} = \left(I + \frac{\Delta x^2}{12}D_x^2 + \frac{\Delta y^2}{12}D_y^2\right)\left[2V_{j,k}^{n+\frac{1}{2}}\psi_{j,k}^{n+\frac{1}{2}} - 2iD_t^+\psi_{j,k}^n\right], \tag{11}$$

with $j,k\in\mathbb{Z}$, $n\geq 0$. Here, we make use of the following difference operators

$$\begin{aligned} D_t^+\psi_{j,k}^n &:= \frac{\psi_{j,k}^{n+1} - \psi_{j,k}^n}{\Delta t}, \\ D_x^2\,\psi_{j,k}^n &:= \frac{\psi_{j-1,k}^n - 2\psi_{j,k}^n + \psi_{j+1,k}^n}{\Delta x^2}, \\ D_y^2\,\psi_{j,k}^n &:= \frac{\psi_{j,k-1}^n - 2\psi_{j,k}^n + \psi_{j,k+1}^n}{\Delta y^2}, \\ \widetilde{D}^2 &:= D_x^2 + D_y^2 + \frac{\Delta x^2 + \Delta y^2}{12}D_x^2\,D_y^2, \end{aligned}$$

the identity operator I, and the abbreviations

$$\psi_{j,k}^{n+\frac{1}{2}} := \frac{1}{2}\left(\psi_{j,k}^{n+1} + \psi_{j,k}^n\right), \qquad V_{j,k}^{n+\frac{1}{2}} := V\left(x_j, y_k, t_{n+\frac{1}{2}}\right).$$

It can be shown by Taylor series that the compact difference scheme (11) approximates the scaled Schrödinger equation (10) with the order $\mathcal{O}(\Delta x^4 + \Delta y^4 + \Delta t^2)$.

Theorem 3.1 (preservation of ℓ^2-norm, [33]) *Let the grid function $V^{n+\frac{1}{2}}$ be bounded for all $n \in \mathbb{N}_0$. For the whole space problems of the 2D time-dependent Schrödinger equation the scheme* (11) *then preserves the ℓ^2-norm*

$$\|\psi^n\|_{\ell^2(\mathbb{Z}^2)} := \sqrt{\Delta x \Delta y \sum_{j,k\in\mathbb{Z}} |\psi^n_{j,k}|^2} \tag{12}$$

in time.

3.2 Derivation of DTBCs for the two dimensional Schrödinger equation

Here, we review the results obtained in [33]. First, we consider the scaled Schrödinger equation

$$\begin{aligned} i\frac{\partial}{\partial t}\psi(x,y,t) &= -\frac{1}{2}\Delta\psi(x,y,t) + V(x,y,t)\psi(x,y,t), \quad (x,y)\in\Omega,\ t>0,\\ \psi(x,y,0) &= \psi^I(x,y), \qquad (x,y)\in\Omega,\\ \psi(x,0,t) &= \psi(x,Y,t) = 0, \qquad x\in\mathbb{R},\ t>0, \end{aligned} \tag{13}$$

on the infinite stripe $\Omega = \mathbb{R}\times(0,Y)$ with some $Y>0$ (cf. Fig. 1). Let the initial function $\psi^I \in L^2(\Omega)$ be compactly supported on the computational domain $\tilde{\Omega}$:

$$\text{supp } \psi^I(x,y) \subset (0,X)\times(0,Y) =: \tilde{\Omega}.$$

Remark 3.2 *For the case that the initial data $\psi^I(x,y)$ is not compactly supported inside the computational domain $\tilde{\Omega}$ we refer the reader to [21].*

The potential $V(x,y,t)$ is assumed to be an $L^\infty(\tilde{\Omega}\times\mathbb{R}^+)$ function in space and time, and constant on each of the two exterior domains $\Omega^C := \Omega\backslash\tilde{\Omega}$. DTBCs will now be derived at the boundaries $x=0$ and $x=X$ of the computational domain $\tilde{\Omega}$.

We introduce the uniform grid $\Omega_{\Delta x,\Delta y} := \{(j\Delta x, k\Delta y)\,|\, j\in\mathbb{Z};\ k=0,\dots,K\in\mathbb{N}\}$ with $x_J = X$, $y_K = Y$ and use the time steps $t_n = n\Delta t$, $n\in\mathbb{N}$. We approximate the TDSE (13) by the difference equation (11). Adapting the continuous strategy and the idea from [8] we take the explicit discrete solution on the exterior domain to eliminate the exterior problem. This is done using first a *discrete sine–transformation*

$$\widehat{\psi}^n_{j,m} := \frac{2}{K}\sum_{k=1}^{K-1}\psi^n_{j,k}\,\sin\left(\frac{\pi k\, m}{K}\right), \qquad m=1,\dots,K-1, \tag{14}$$

in y-direction and then a $\mathcal{Z}$-transformation

$$\mathcal{Z}\left(\widehat{\psi}^n_{j,m}\right) := \Phi_{j,m}(z) := \sum_{n=0}^{\infty}\widehat{\psi}^n_{j,m}z^{-n} \quad \text{with } z\in\mathbb{C},\ |z|>1, \tag{15}$$

in the discrete time variable. The sine–transformed scheme (11) for the modes $\widehat{\psi}^n_{j,m}$, $m = 1, \ldots, K-1$, $j \leq 0$ and $j \geq J$ reads

$$\begin{aligned}\gamma_m\, \widehat{\psi}^{n+1}_{j+1,m} + \gamma_m\, \widehat{\psi}^{n+1}_{j-1,m} + \rho_m\, \widehat{\psi}^{n+1}_{j,m} \\ = (2W - \gamma_m)\, \widehat{\psi}^n_{j+1,m} + (2W - \gamma_m)\, \widehat{\psi}^n_{j-1,m} + (\kappa_m - \rho_m)\, \widehat{\psi}^n_{j,m},\end{aligned} \tag{16}$$

where we use the abbreviations

$$\begin{aligned} D &:= \frac{\Delta x^2}{\Delta y^2}, \qquad C := \frac{\Delta x^2 + \Delta y^2}{12\Delta y^2}, \qquad W := \frac{i\Delta x^2}{3\Delta t}, \\ \gamma_{j,m} &:= 1 + 2C\left(\cos\left(\frac{\pi m}{K}\right) - 1\right) + W - \frac{\Delta x^2}{6} V_j, \\ \kappa_m &:= 4\left(\cos\left(\frac{\pi m}{K}\right) + 4\right) W, \\ \rho_{j,m} &:= -2 - 2D + 4C + 8W - \frac{4\Delta x^2}{3} V_j \\ &\quad + \left(2D - 4C + 2W - \frac{\Delta x^2}{3} V_j\right) \cos\left(\frac{\pi m}{K}\right), \end{aligned} \tag{17}$$

$m = 1, \ldots, K-1$, and V_j denotes the constant potential on Ω^C, which may take different values (i.e. V_0, V_J) on each outer domain. Performing the $\mathcal{Z}$–transformation of (16) we obtain

$$\Phi_{j+1,m}(z) + \left[\frac{\rho_{j,m}(z+1) - \kappa_m}{\gamma_{j,m}(z+1) - 2W}\right] \Phi_{j,m}(z) + \Phi_{j-1,m}(z) = 0, \tag{18}$$

$j \leq 0$, $j \geq J$, $m = 1, \ldots, K-1$. Note that the coefficients are constant in j on each part of the outer domain. For the derivation of (18) we have used the fact that the initial function has compact support on the computational domain, hence

$$\widehat{\psi}^0_{j+1,m} = \widehat{\psi}^0_{j-1,m} = \widehat{\psi}^0_{j,m} = 0, \qquad m = 1, \ldots, K-1,\ j = 0, J.$$

With the physical constraint that the solution $\psi^n_{j,k}$ of (11) decays for $|j| \to \infty$ we calculate the unique solution $\Phi_{j,m}(z) = (\nu_{J,m}(z))^j$ of equation (18). $\nu_{J,m}(z)$ denotes that solution of the characteristic equation

$$(\nu_{J,m}(z))^2 + \left[\frac{\rho_{J,m}(z+1) - \kappa_m}{\gamma_{J,m}(z+1) - 2W}\right] \nu_{J,m}(z) + 1 = 0,$$

which satisfies $|\nu_{J,m}(z)| < 1$. We note that this is always possible for $|z| > 1$. $\Phi_{j,m}(z)$ then fulfills the $\mathcal{Z}$-transformed DTBCs at $j = 0,\ J$ for each mode:

$$\Phi_{1,m}(z) = \frac{1}{\nu_{0,m}(z)} \Phi_{0,m}(z), \tag{19a}$$

$$\Phi_{J-1,m}(z) = \frac{1}{\nu_{J,m}(z)} \Phi_{J,m}(z), \tag{19b}$$

with

$$\nu_{j,m}(z) = \frac{-\rho_{j,m}(z+1) + \kappa_m + \sqrt{\zeta_{j,m} z^2 - 2\xi_{j,m} z + \theta_{j,m}}}{2\gamma_{j,m}(z - \eta_{j,m})}, \quad j = 0, J. \tag{20}$$

Here we use that branch of the square root, which yields $|\nu_{j,m}(z)| < 1$ and we introduce the abbreviations

$$\begin{aligned} \eta_{j,m} &:= \frac{2W}{\gamma_{j,m}} - 1, \\ \zeta_{j,m} &:= (\rho_{j,m})^2 - 4(\gamma_{j,m})^2, \\ \theta_{j,m} &:= (\kappa_m - \rho_{j,m})^2 - 4(\gamma_{j,m}\eta_{j,m})^2, \\ \xi_{j,m} &:= -(\rho_{j,m})^2 - 4(\gamma_{j,m})^2 \eta_{j,m} + \rho_{j,m}\kappa_m, \end{aligned} \tag{21}$$

$m = 1, \dots, K-1$. With some tedious work one can calculate analytically the $\mathcal{Z}$-inverse of (20): $\mathcal{Z}^{-1}(\nu_{j,m}(z))^{(n)} =: \ell_{j,m}^{(n)}$. We use the auxiliary function

$$F(z, \mu_{j,m}) := \frac{z}{\sqrt{z^2 - 2\mu_{j,m} z + 1}},$$

with

$$\mu_{j,m} := \frac{\xi_{j,m}}{\sqrt{\zeta_{j,m}}\sqrt{\theta_{j,m}}}, \qquad m = 1, \dots, K-1. \tag{22}$$

Using the abbreviations

$$\begin{aligned} \lambda_{j,m} &:= \frac{\sqrt{\zeta_{j,m}}}{\sqrt{\theta_{j,m}}}, \\ \tau_{j,m} &:= \frac{\theta_{j,m}}{\eta_{j,m}} - \zeta_{j,m}\eta_{j,m} - 2\xi_{j,m}, \qquad m = 1, \dots, K-1, \end{aligned} \tag{23}$$

we obtain

$$\frac{\sqrt{\zeta_{j,m} z^2 - 2\xi_{j,m} z + \theta_{j,m}}}{z - \eta_{j,m}} = \frac{1}{\sqrt{\zeta_{j,m}}} \Big(\zeta_{j,m} - \frac{\theta_{j,m}}{z\eta_{j,m}} + \frac{\tau_{j,m}}{z - \eta_{j,m}} \Big) F(z, \mu_{j,m})$$

by comparison of coefficients. Hence, we have

$$\begin{aligned} \nu_{j,m}(z) = &-\frac{\rho_{j,m}}{2\gamma_{j,m}} \frac{z}{z - \eta_{j,m}} - \frac{\rho_{j,m} - \kappa_m}{2\gamma_{j,m}} \frac{1}{z - \eta_{j,m}} \\ &+ \frac{1}{2\gamma_{j,m}} \frac{1}{\sqrt{\zeta_{j,m}}} \Big(\zeta_{j,m} - \frac{\theta_{j,m}}{z\eta_{j,m}} + \frac{\tau_{j,m}}{z - \eta_{j,m}} \Big) F(z, \mu_{j,m}), \end{aligned}$$

and its inverse $\mathcal{Z}$–transform $\ell_{j,m}^{(n)} = \left(\mathcal{Z}^{-1}\left[\frac{1}{\nu_{j,m}(z)}\right]\right)_n$ reads

$$\ell_{j,m}^{(n)} = -\frac{\rho_{j,m}}{2\gamma_{j,m}}\eta_{j,m}^n - \frac{\rho_{j,m}-\kappa_m}{2\gamma_{j,m}}\left(\eta_{j,m}^{n-1} - \frac{1}{\eta_{j,m}}\delta_n^0\right) + \frac{\sqrt{\theta_{j,m}}}{2\gamma_{j,m}}\Big[\lambda_{j,m}^{1-n}P_n(\mu_{j,m}) - \frac{1}{\eta_{j,m}}\lambda_{j,m}^{-n}P_{n-1}(\mu_{j,m}) + \frac{\tau_{j,m}}{\eta_{j,m}\sqrt{\theta_{j,m}\zeta_{j,m}}}\sum_{k=0}^{n-1}(\lambda_{j,m}\eta_{j,m})^n P_k(\mu_{j,m})\Big],\ n\in\mathbb{N}_0, \tag{24}$$

with the Legendre polynomials P_n ($P_{-1}\equiv 0$), the Kronecker symbol δ_n^0, and the abbreviations used in (17), (21), (22) and (23). The sine-transformed DTBCs at $j=0$ and $j=J$ for the 2D discrete Schrödinger (11) follow with the inverse $\mathcal{Z}$-transformation of (19):

$$\widehat{\psi}_{1,m}^n - \ell_{0,m}^{(0)}\widehat{\psi}_{0,m}^n = \sum_{p=1}^{n-1}\ell_{0,m}^{(n-p)}\widehat{\psi}_{0,m}^p, \quad n\geq 1, \tag{25a}$$

$$\widehat{\psi}_{J-1,m}^n - \ell_{J,m}^{(0)}\widehat{\psi}_{J,m}^n = \sum_{p=1}^{n-1}\ell_{J,m}^{(n-p)}\widehat{\psi}_{J,m}^p, \quad n\geq 1. \tag{25b}$$

Remark 3.3 *The convolution coefficients $\ell_{j,m}^{(n)}$ are highly oscillatory as a function of the time step n. In [33] it is shown that the convolution coefficients $\ell_{j,m}^{(n)}$ given in* (24) *have the asymptotic behaviour*

$$\ell_{j,m}^{(n)} \sim \sigma_{j,m}\, e^{i\vartheta_{j,m}n} \tag{26}$$

as $n\to\infty$, with

$$\sigma_{j,m} := -\frac{\rho_{j,m}}{2\gamma_{j,m}} + \frac{\kappa_m-\rho_{j,m}}{2\gamma_{j,m}\eta_{j,m}} + \frac{\sqrt{\tau_{j,m}}}{2\gamma_{j,m}\sqrt{\eta_{j,m}}}, \quad \vartheta_{j,m} = \arg(\eta_{j,m})$$

for $j=0,\ J$ and $m=1,\dots,K-1$. This behaviour deviates from the $\mathcal{O}(t^{-3/2})$–decay of the continuous convolution kernel in (7)*. Hence, it may lead to numerical cancellations in the calculation of the convolution sums* (25)*. As an alternative we shall derive coefficients that decay like $\mathcal{O}(n^{-3/2})$. For the left DTBCs we therefore add equation* (25a) *for n and $n+1$ with the corresponding weighting factor 1 and $-e^{i\vartheta_{1,m}} = -\eta_{1,m}$ (the case $j=J$ is analogous) and proceed like in [17]. We define the* summed coefficients

$$s_{j,m}^{(n)} := \begin{cases} \ell_{j,m}^{(n)} - \eta_{j,m}\,\ell_{j,m}^{(n-1)}, & n\geq 1,\\ \ell_{j,m}^{(0)}, & n=0, \end{cases} \tag{27}$$

for $m=1,\dots,K-1$; $j=0$ and $j=J$. In Fig. 4 we give an example on the asymptotic behaviour of the convolution coefficients. The free Schrödinger equation is discretized with $J=K=50$, $\Delta x=\Delta y=0.02$ and $\Delta t = 2\cdot 10^{-5}$. A solution ψ is calculated for

$n = 1, \dots, 250$ *time steps. In Fig. 4(a) we present the real part of* $\ell_{J,m}^{(n)}$ *and the absolute value* $|\ell_{J,m}^{(n)}|$ *in Fig. 4(b) for all modes* $m = 1, \dots, K-1$. *The errors* $\mathrm{Re}\,(\sigma_{J,m}e^{i\vartheta n} - \ell_{J,m}^{(n)})$ *and* $|\sigma_{J,m}e^{i\vartheta n} - \ell_{J,m}^{(n)}|$ *between the convolution coefficients and the asymptotic expression* (26) *– which are converging to zero – are shown in Fig. 4(c) and Fig. 4(d).*

Theorem 3.4 (DTBCs for the 2D Schrödinger equation, [33]) *The sine-transformed DTBCs at* $j = 0$ *and* $j = J$ *for the discrete Schrödinger equation* (11) *read*

$$\widehat{\psi}_{1,m}^n - s_{0,m}^{(0)}\widehat{\psi}_{0,m}^n = \sum_{p=1}^{n-1} s_{0,m}^{(n-p)}\widehat{\psi}_{0,m}^p + \eta_{1,m}\widehat{\psi}_{1,m}^{n-1}, \tag{28a}$$

$$\widehat{\psi}_{J-1,m}^n - s_{J,m}^{(0)}\widehat{\psi}_{J,m}^n = \sum_{p=1}^{n-1} s_{J,m}^{(n-p)}\widehat{\psi}_{J,m}^p + \eta_{J-1,m}\widehat{\psi}_{J-1,m}^{n-1}. \tag{28b}$$

The coefficients $s_{j,m}^{(n)}$ *for* $j = 0, J$, $m = 1, \dots, K-1$ *are given by equation* (27). *For* $n \geq 2$, *they can be calculated by the formula*

$$s_{j,m}^{(n)} = -\frac{\sqrt{\theta_{j,m}}}{2\gamma_{j,m}}\lambda_{j,m}^{1-n}\,\frac{P_n(\mu_{j,m}) - P_{n-2}(\mu_{j,m})}{2n-1}, \tag{29}$$

or by the recursion

$$s_{j,m}^{(n+1)} = \frac{2n-1}{n+1}\frac{\mu_{j,m}}{\lambda_{j,m}}s_{j,m}^{(n)} - \frac{n-2}{n+1}(\lambda_{j,m})^{-2}s_{j,m}^{(n-1)}, \tag{30}$$

for $j = 0,\ J$ *and* $m = 1, \dots, K-1$. *These new coefficients have the asymptotic behaviour*

$$s_{j,m}^{(n)} \sim \mathcal{O}(n^{-3/2}). \tag{31}$$

Remark 3.5 *The idea of deriving DTBCs is to eliminate the exterior problem by using the explicit solution on the outer domain* Ω^C. *This is the reason for assuming a uniform grid on the exterior domain* Ω^C. *On the computational domain* $\tilde{\Omega}$, *however, the grid can be non–uniform, or even adaptive in time.*

Remark 3.6 *Recently, it was discovered by the authors that a more convenient formulation of* (19) *is given by*

$$\nu_{0,m}(z)\Phi_{1,m}(z) = \Phi_{0,m}(z), \quad \nu_{J,m}(z)\Phi_{J-1,m}(z) = \Phi_{J,m}(z).$$

Here, the inverse $\mathcal{Z}$*-transformation of* $\nu_{j,m}(z)$, $j = 0, J$ *already decays like* $\mathcal{O}(n^{-3/2})$. *Instead of* (28), *this approach yields DTBCs with discrete convolutions at the 'interior' grid points* $j = 1,\ J-1$ *(cf. [9] for details).*

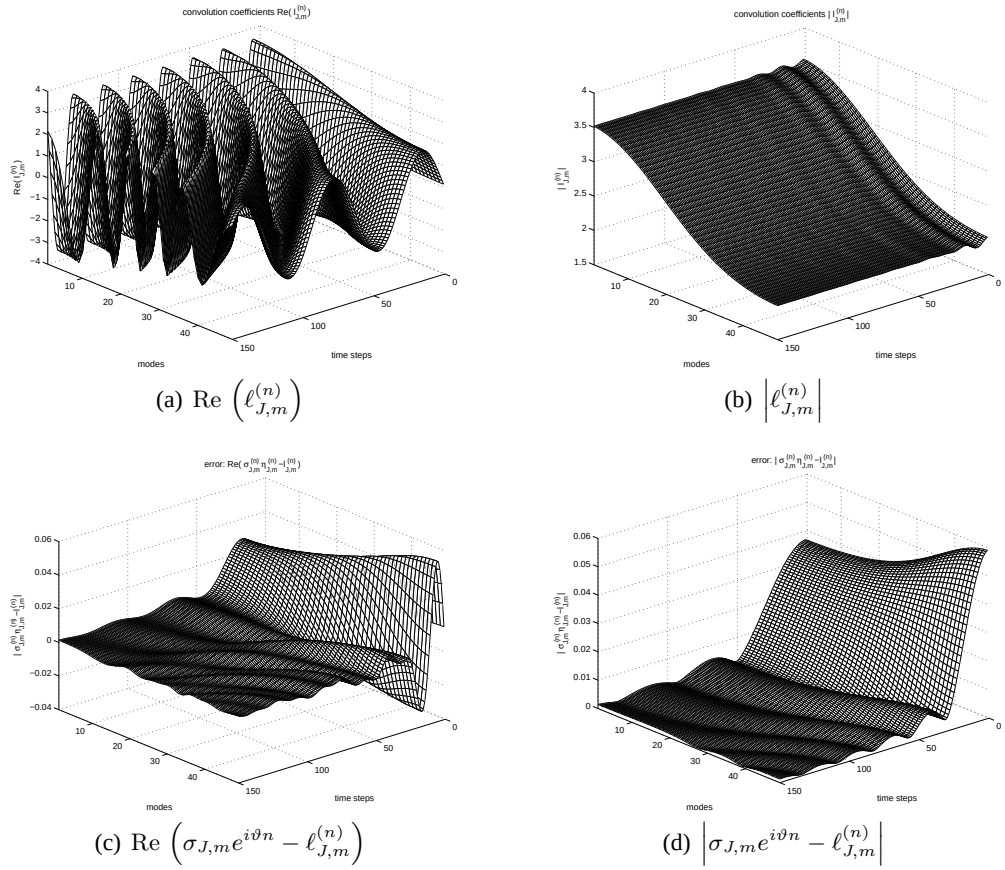

(a) $\mathrm{Re}\left(\ell_{J,m}^{(n)}\right)$ (b) $\left|\ell_{J,m}^{(n)}\right|$

(c) $\mathrm{Re}\left(\sigma_{J,m}e^{i\vartheta n} - \ell_{J,m}^{(n)}\right)$ (d) $\left|\sigma_{J,m}e^{i\vartheta n} - \ell_{J,m}^{(n)}\right|$

Figure 4: Real part (a) and absolute value (b) of the convolution coefficients $\ell_{J,m}^{(n)}$ and real part (c) and absolute value (d) of the error $\sigma_{J,m}e^{i\vartheta n} - \ell_{J,m}^{(n)}$ between the asymptotic expansion (26) and the convolution coefficients for the modes $m = 1, \ldots, K-1$ as a function of the time steps $n = 1, \ldots, 250$. We consider the computational domain $\tilde{\Omega} = (0,1) \times (0,1)$ and choose the discretization parameters $J = K = 50$, $\Delta x = \Delta y = 0.02$ and $\Delta t = 2 \cdot 10^{-5}$.

3.3 Approximation of the DTBCs by Sums of Exponentials

An ad-hoc implementation of the discrete convolution at the right boundary $x_J = X$

$$\sum_{p=1}^{n-1} s_{J,m}^{(n-p)} \widehat{\psi}_{J,m}^{p}, \qquad m = 1, \dots, K-1$$

in (28b) with convolution coefficients $s_{J,m}^{(n)}$ from (27) has still one disadvantage. The boundary conditions of this kind are non–local both in time and space (w.r.t. the y-direction) and therefore computations are too expensive. As a remedy, to get rid of this time non–locality, we proposed already in [8] the *sum of exponentials ansatz*, i.e. to approximate the kernel (27) by a finite sum (say L terms) of exponentials that *decay* with respect to time. This approach allows for a fast (approximate) evaluation of the discrete convolution in (28b) since the convolution can now be evaluated with a simple recurrence formula for L auxiliary terms and the numerical effort now remains constant in time. On the Laplace–transformed level this approximation amounts to replace the symbol $\hat{s}_{J,m}(z) = \frac{z-\eta_{J,m}}{z}\nu_{J,m}(z)$ (cf. (27)) of the convolution by a rational approximation.

In the sequel we will briefly review this ansatz [8]. In order to derive a fast numerical method to calculate the discrete convolution in (28b), we approximate the coefficients $s_{J,m}^{(n)}$ for each mode m by the following ansatz (*sum of exponentials*):

$$s_{J,m}^{(n)} \approx \tilde{s}_{J,m}^{(n)} := \begin{cases} s_{J,m}^{(n)}, & n = 0, 1, \dots, \upsilon_m - 1 \\ \displaystyle\sum_{l=1}^{L_m} b_{m,l} q_{m,l}^{-n}, & n = \upsilon_m, \upsilon_m + 1, \dots, \end{cases} \tag{32}$$

where $L_m, \upsilon_m \in \mathbb{N}$ are a fixed numbers. Evidently, the approximation properties of $\tilde{s}_{J,m}^{(n)}$ depend on L_m, υ_m, and the corresponding set $\{b_{m,l}, q_{m,l}\}$. Thus, the choice of an (in some sense) optimal approximation would be a difficult nonlinear problem, which we do not pursue here. Instead, we propose below a deterministic method of finding $\{b_{m,l}, q_{m,l}\}$ for fixed L_m, υ_m and for each mode m.

The "split" definition of $\{\tilde{s}_{J,m}^{(n)}\}$ in (32) is motivated by the fact that the implementation of the right discrete TBC (28b) involves a convolution sum with p ranging only from 1 to $p = n-1$. Since the first coefficient $s_{J,m}^{(0)}$ does not appear in this convolution, it makes no sense to include it in our sum of exponential approximation, which aims at simplifying the evaluation of the convolution. Hence, one may choose $\upsilon_m = 1$ in (32). The "special form" of $\ell_{J,m}^{(0)}$ and $\ell_{J,m}^{(1)}$ given in [8] suggests even to exclude $s_{J,m}^{(1)}$ from this approximation and to choose $\upsilon_m = 2$ in (32). We use this latter choice in our numerical implementation in the Example in the following §4.

Also, there is an additional motivation for choosing $\upsilon_m = 2$: With the choice $\upsilon_m = 0$ (or $\upsilon_m = 1$) we typically obtain (for each mode) two (or, resp., one) coefficient pairs $(b_{m,l}, q_{m,l})$ of big magnitude. These "outlier" values reflect the different nature of the first

two coefficients. Including them into our discrete sum of exponentials would then yield less accurate approximation results.

Let us fix L_m and consider the formal power series:

$$g_m(x) := s_{J,m}^{(\upsilon_m)} + s_{J,m}^{(\upsilon_m+1)} x + s_{J,m}^{(\upsilon_m+2)} x^2 + \ldots, \quad |x| \leq 1. \tag{33}$$

If there exists the $[L_m - 1|L_m]$ *Padé approximation*

$$\tilde{g}_m(x) := \frac{P_{L_m-1}(x)}{Q_{L_m}(x)}$$

of (33), then its Taylor series

$$\tilde{g}_m(x) = \tilde{s}_{J,m}^{(\upsilon_m)} + \tilde{s}_{J,m}^{(\upsilon_m+1)} x + \tilde{s}_{J,m}^{(\upsilon_m+2)} x^2 + \ldots$$

satisfies the conditions

$$\tilde{s}_{J,m}^{(n)} = s_{J,m}^{(n)}, \qquad n = \upsilon_m, \upsilon_m + 1, \ldots, 2L_m + \upsilon_m - 1, \tag{34}$$

due to the definition of the Padé approximation rule.

Theorem 3.7 ([8]) *Let $Q_{L_m}(x)$ have L_m simple roots $q_{m,l}$ with $|q_{m,l}| > 1, \quad l = 1, \ldots, L_m$. Then*

$$\tilde{s}_{J,m}^{(n)} = \sum_{l=1}^{L_m} b_{m,l} q_{m,l}^{-n}, \qquad n = \upsilon_m, \upsilon_m + 1, \ldots, \tag{35}$$

where

$$b_{m,l} := -\frac{P_{L_m-1}(q_{m,l})}{Q'_{L_m}(q_{m,l})}\, q_{m,l} \neq 0, \qquad l = 1, \ldots, L_m. \tag{36}$$

Remark 3.8 *Let us note that the assumption in Theorem 3.7 on the roots of $Q_{L_m}(x)$ to be simple is not essential. For multiple roots one only has to reformulate Theorem 3.7. All our practical calculations confirm that this assumption holds for any desired L_m, although we cannot prove this.*

Evidently, the approximation to the convolution coefficients $s_{J,m}^{(n)}$ by the representation (32) using a $[L_m - 1|L_m]$ Padé approximant to (33) behaves as follows: the first $2L_m$ coefficients are reproduced exactly, see (34). However, the asymptotic behaviour of $s_{J,m}^{(n)}$ and $\tilde{s}_{J,m}^{(n)}$ (as $n \to \infty$) differ strongly – algebraic versus exponential decay.

3.4 Fast Evaluation of the Discrete Convolution.

Let us consider the approximation (32) of the discrete convolution kernel appearing in the right discrete TBC (28b). With these "exponential" coefficients the *approximated convolution*

$$\tilde{C}_{J,m}^{(n-1)} := \sum_{p=1}^{n-1} \tilde{s}_{J,m}^{(n-p)} \widehat{\psi}_{J,m}^{p}, \qquad \tilde{s}_{J,m}^{(n)} = \sum_{l=1}^{L_m} b_{m,l} q_{m,l}^{-n}, \tag{37}$$

$|q_{m,l}| > 1$, of a discrete function $\widehat{\psi}_{J,m}^{p}$, $p = 1, 2, \ldots$, with the kernel coefficients $\tilde{s}_{J,m}^{(n)}$, can be calculated by recurrence formulas, and this will reduce the numerical effort significantly.

A straightforward calculation (cf. [8]) yields: The value $\tilde{C}_{J,m}^{(n-1)}$ from (37) for $n \geq 2$ is represented by

$$\tilde{C}_{J,m}^{(n-1)} = \sum_{l=1}^{L_m} \tilde{c}_{J,m,l}^{(n-1)}, \tag{38}$$

where

$$\tilde{c}_{J,l,m}^{(0)} \equiv 0,$$

$$\tilde{c}_{J,m,l}^{(n-1)} = q_{m,l}^{-1} \tilde{c}_{J,m,l}^{(n-2)} + b_{m,l} q_{m,l}^{-\nu_m} \psi_{J+1,m}^{n-2}, \tag{39}$$

$n = 2, 3, \ldots$, $l = 1, \ldots, L_m$.

Remark 3.9 (Transformation of approximated convolution coefficients, [8]) *Let $\upsilon_m = 2$. Let the approximated convolution coefficients $\tilde{s}_{J,m}^{(n)}$ and the coefficient pairs $\{b_{m,l},\, q_{m,l}\}$ from Theorem 3.7 be given for a set $\{\Delta x, \Delta y, \Delta t, V\}$ for all modes $m = 1, \ldots, K-1$. Then, define for another parameter set $\{\Delta x^*, \Delta y^*, \Delta t^*, V^*\}$ the coefficients $\{b_{m,l}^*,\, q_{m,l}^*\}$ given by*

$$\begin{aligned}
q_{m,l}^* &:= \frac{q_{m,l}\bar{a}_m - \bar{b}_m}{a_m - q_{m,l} b_m}, \\
b_{m,l}^* &:= b_{l,m} q_{m,l} \frac{a_m \bar{a}_m - b_m \bar{b}_m}{(a_m - q_{m,l} b_m)(q_{m,l}\bar{a}_m - \bar{b}_m)} \frac{1 + q_{m,l}^*}{1 + q_{m,l}}, \\
a_m &:= 2\frac{\Delta x^2}{\Delta t} + 2\frac{(\Delta x^*)^2}{\Delta t^*} + i(\Delta x^2 V - (\Delta x^*)^2 V^*), \\
b_m &:= 2\frac{\Delta x^2}{\Delta t} - 2\frac{(\Delta x^*)^2}{\Delta t^*} - i(\Delta x^2 V - (\Delta x^*)^2 V^*).
\end{aligned}$$

The resulting convolution coefficients $\left(\tilde{s}_{J,m}^{(n)}\right)^*$ (obtained via (37)) are in practise good approximations for $\left(s_{J,m}^{(n)}\right)^*$, the exact convolution coefficients for the parameters $\{\Delta x^*, \Delta y^*, \Delta t^*, V^*\}$ (cf. (29) or (30)).

Finally we summarize the sum-of-exponentials approach by the following algorithm. For each mode $m = 1, \ldots, K-1$:

1. Prescribe L_m, ν_m, take $\Delta x = \Delta y = \Delta t = 1$ and calculate the coefficients $s_{J,m}^{(n)}$, $n = \nu_m, \nu_m + 1, \ldots, 2L_m + \nu_m - 1$ with (29) or (30).

2. Calculate $\{b_{m,l},\, q_{m,l}\}$ and $\tilde{s}_{J,m}^{(n)}$ via Padé–algorithm.

3. For given Δx^*, Δy^*, Δt^*, V^* use Remark 3.9 with $\Delta x = \Delta y = \Delta t = 1$ and $\{b_{m,l},\, q_{m,l}\}$ for the computation of $\{b_{m,l}^*,\, q_{m,l}^*\}$.

4. The corresponding coefficients $b_{m,l}$, $q_{m,l}$ are used for the computation of $\tilde{s}_{J,m}^{(n)}$ and for the efficient calculation of the discrete convolutions.

Steps 1 and 2 are made once and for all, see [8] for tables of coefficient pairs $\{b_{m,l},\, q_{m,l}\}$ or `http://www.dtbc.de.vu/` for the implemented Padé algorithm (Maple code).

3.5 Implementation of the DTBCs

In (28) the DTBCs are written in sine–transformed space. A direct implementation in position space would necessitate tremendous numerical costs, hence they are implemented in y sine-transformed space (cf. [10]). The discrete convolution

$$\widehat{C}_{J,m}^{(n-1)} := \sum_{p=1}^{n-1} s_{J,m}^{(n-p)} \widehat{\psi}_{J,m}^{p}, \quad m = 1, \ldots, K-1 \tag{40}$$

for the right boundary $x_J = J\Delta x$ is calculated in sine-transformed space and inverse transformed by

$$C_{J,k}^{(n-1)} = 2 \sum_{m=1}^{K-1} \sin\left(\frac{\pi m k}{K}\right) \Big(\sum_{p=1}^{n-1} s_{J,m}^{(n-p)} \widehat{\psi}_{J,m}^{p} \Big), \quad k = 1, \ldots, K-1.$$

Since the convolution (40) only involves the solution at the boundary at past time levels (i.e. for $p \le n-1$), one can directly store the sine-transformed boundary data $\widehat{\psi}_{J,m}^{p}$. Moreover, this part of the DTBCs only enters the inhomogeneity of the linear system to be solved at each time level.

The part $s_{J,m}^{(0)} \widehat{\psi}_{J,m}^{n}$ of the left hand side of the DTBCs (28b) has to be inverse transformed to physical space and we get the couplings

$$\begin{aligned} \Big(s_{J,m}^{(0)} \widehat{\psi}_{J,m}^{n} \Big)_{J,k,l}^{\vee} &= 2 \sum_{m=1}^{K-1} \sin\left(\frac{\pi m k}{K}\right) s_{J,m}^{(0)} \widehat{\psi}_{J,m}^{n} \\ &= \frac{2}{K} \sum_{m=1}^{K-1} \sum_{l=1}^{K-1} s_{J,m}^{(0)} \sin\left(\frac{\pi m k}{K}\right) \sin\left(\frac{\pi k l}{K}\right) \psi_{J,l}^{n} \end{aligned}$$

for $k,\, l = 1, \ldots, K-1$. Hence, the 9-diagonal system of the discrete 2D Schrödinger equation (11) obtains additional entries due to the DTBCs.

In order to model the electron influx from the left lead, we shall prescribe an incoming plane wave $\varphi(x,y,t)$ at the left boundary. Hence, inhomogeneous DTBCs have to be used at $x_0 = 0$:

$$\widehat{\psi}^n_{1,m} - \widehat{\varphi}^n_{1,m} - s^{(0)}_{0,m}\left(\widehat{\psi}^n_{0,m} - \widehat{\varphi}^n_{0,m}\right) = \sum_{p=1}^{n-1} s^{(n-p)}_{0,m}\left(\widehat{\psi}^p_{0,m} - \widehat{\varphi}^p_{0,m}\right) - \eta_{1,m}\left(\widehat{\psi}^{n-1}_{1,m} - \widehat{\varphi}^{n-1}_{1,m}\right), \quad n \geq 1, \quad (41)$$

with the discrete, sine-transformed incoming wave $\varphi^n_{j,k}$, $0 \leq k \leq K, 0 \leq j \leq J$. These boundary conditions are implemented analogously to the right DTBCs at $x_J = X$.

4 Numerical results

In this section we first present some rather mathematical examples on DTBCs for the Schrödinger equation in two dimensions. We verify numerically the accuracy of the DTBCs for the free Schrödinger equation. Then we apply the DTBCs to the simulation of quantum waveguides.

4.1 Travelling Gaussian wave functions

In this first example we solve the two dimensional, transient Schrödinger equation (1) discretized with the compact nine-point scheme (11) on the time-constant domain $\Omega = (0,1)^2$. As an initial function we choose the y-periodic Gaussian wave function

$$\psi^I(x,y) = \sum_{\ell\in\mathbb{Z}} (-1)^\ell e^{-\frac{\alpha}{2}\left[(x-x_0)^2+(y-y_0+\ell)^2\right]+ik_x x+ik_y y}, \quad (x,y)\in\Omega \quad (42)$$

with the parameters $\alpha = 240$, $x_0 = 3/4$, and $y_0 = 1/4$. As specified by the wave numbers $k_x = 140$, $k_y = 120$ the resulting wave has a non–orthogonal impact on the boundary (cf. Fig. 5 (b-d)). This is typically a "rough test" for TBCs, as high orthogonal solution modes then become significally coupled into the system. Exact DTBCs according to (28) are implemented at $x = 0$, $x = 1$. We consider the discretization parameters $\Delta x = \Delta y = 1/120$, $\Delta t = 2\cdot 10^{-5}$. In Figure 5(a) we show the absolute value of the initial function (42). The evolution of this initial function according to the Schrödinger equation is presented in Figure 5 (b), (c), (d) for some times t_n. The Gaussian beam leaves the computational domain through the artificial boundary $x = 1$ without being reflected back. For the determination of the error due to the artificial boundary conditions we compare the numerical solution ψ with a numerical reference solution $\tilde{\psi}$ on $\tilde{\Omega} = (0,2)\times(0,1)$. The reference solution is calculated with the same discretization scheme, and with DTBCs at $x = 0$, $x = 2$. We obtain the relative L^2-error

$$L(t) = \frac{||\psi(.,.,t) - \tilde{\psi}(.,.,t)||_{\ell^2(\Omega)}}{||\psi^I(.,.)||_{\ell^2(\Omega)}}. \quad (43)$$

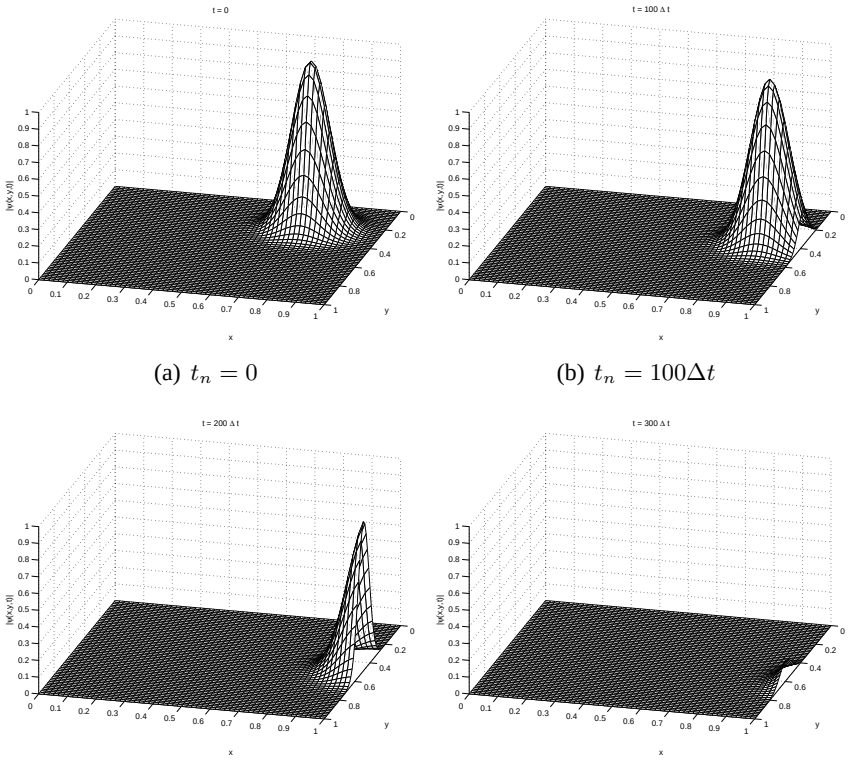

(a) $t_n = 0$ (b) $t_n = 100\Delta t$

(c) $t_n = 200\Delta t$ (d) $t_n = 300\Delta t$

Figure 5: Absolute value of the initial function (42) and the absolute value of the solution to the Schrödinger equation at some time steps t_n calculated with exact DTBCs at $x = 0$ and $x = 1$. The wave impinges on the boundary at a non–orthogonal angle. The discretization parameters are $\Delta x = \Delta y = 1/120$ and $\Delta t = 2 \cdot 10^{-5}$.

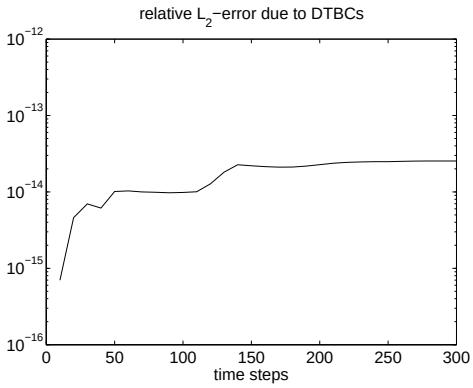

Figure 6: Relative error $L(\psi, \tilde{\psi}, t_n)$ due to the boundary conditions.

Within this test the error due to the cut–off of the initial function is also included. The effects of the artificial boundary at $x = 2$ should be negligible here, because ψ essentially does not cross this boundary during the simulation period. In Figure 6 this error $L(t)$ is plotted. We remark that the magnitude of this error is about the rounding error of Matlab.

4.2 Quantum waveguide simulation

Here we will present a physical application of DTBCs. Artificial boundary conditions play an essential role in Schrödinger based simulations of the electron transport through quantum semiconductor devices. Typical examples of practical relevance include the ballistic transport along the channel of MOSFETs (cf. [27], [37]) or quantum waveguides (cf. [13]) for an analysis of T-shaped *quantum interference transistors*. These are novel electronic switches of nano–scale dimensions. They are made of several different layers of semiconductor materials such that the electron flow is confined to small channels or waveguides. Due to their sandwiched structure the relevant geometry for the electron current is essentially two dimensional.

Following the simulation of a GaAs–waveguide in [13], we choose the T–shaped geometry shown in Fig. 2 to simulate a quantum waveguide transistor. In x-direction the channel has a length of $X = 60$nm; the channel width Y and the stub width w are 20nm. In order to control the current through the channel, the stub length can be changed from $L_1 = 32$nm to $L_2 = 40.5$nm. Homogeneous DTBCs are implemented at $x = X$. An inhomogeneous DTBC at $x = 0$ (cf. (41)) models the prescribed influx of electrons. All other boundaries are considered as hard walls, i. e. we use homogeneous Dirichlet boundary conditions for ψ. A (discrete) time harmonic incoming wave function

$$\varphi_{j,k}^n = \sin\left(\frac{\pi k}{K}\right) e^{ik_x j\Delta x} e^{-\frac{iE_x n\Delta t}{\hbar}}, \quad k = 0, \ldots, K \tag{44}$$

is modeling the mono-energetic constant incoming current at $x = 0$. Here, φ includes

only the lowest transversal mode. But any linear combination of higher modes would work equally well, which is a great advantage compared to other artificial boundary conditions (e.g. [13]). In our example the energy E of the incoming wave equals 29.9meV and the effective electron mass has the value $m^* = 0.067m_0$, which corresponds to GaAs. In the subsequent simulations we are mostly interested in the switching and the large time behaviour of this waveguide. Therefore we first need to compute a stationary state corresponding to a given incoming plane wave function ψ^{Inc}. For this initialization process we choose the following (somewhat arbitrary) initial function

$$\psi^I(x,y) = \begin{cases} \sin\left(\frac{y\pi}{Y_1}\right) e^{ik_x x} & 0 \le x < x_1 \\ \frac{1}{2}\sin\left(\frac{y\pi}{Y_1}\right) e^{ik_x x}\left[1+\cos\left(\pi\frac{x-x_1}{x_2-x_1}\right)\right] & x_1 \le x < x_2 \\ 0 & x \ge x_2 \end{cases} \tag{45}$$

with $x_1 = 5$nm and $x_2 = 15$nm, which is consistent with the incoming wave. Then we solve the TDSE until stationarity is reached. The value of k_x can be derived from the discrete dispersion relation.

In the analytic case the dispersion relation for the free Schrödinger equation

$$i\hbar\frac{\partial}{\partial t}\psi \;=\; -\frac{\hbar^2}{2m_*}\Delta\psi + V(x,y,t)\psi, \quad (x,y)\in\Omega,\, t>0\,, \tag{46}$$

on a domain $\mathbb{R}\times(0,Y_1)$ with a plane wave solution in the first orthogonal mode (cf. (44)) reads

$$\epsilon(k_x) = \frac{\hbar^2 k_x^2}{2m_*} + \frac{\hbar^2\pi^2}{2m_* Y_1^2}, \tag{47}$$

which needs to be modified for the discretized Schrödinger equation. For a given inflow energy E, the value of k_x appearing in (45) can be derived from the following *discrete dispersion relation*. To derive it, we first put the ansatz $\psi_{j,1} = e^{ik_x j\Delta x}\sin\left(\frac{\pi\Delta y}{Y_1}\right)$, $j\in\mathbb{Z}$ into the spatial semi-discretization (by the compact nine-point scheme) analogous to (11):

$$\begin{aligned} E_{\mathrm{space}}(k_x) \;=\; & \Big[-\frac{\hbar^2}{m_*\Delta x^2}\left(\cos(k_x\Delta x)-1\right) - \frac{\hbar^2}{m_*\Delta y^2}\left(\cos\left(\frac{\pi\Delta y}{Y_1}\right)-1\right) \\ & -\frac{\hbar^2(\Delta x^2+\Delta y^2)}{6m_*\Delta x^2\Delta y^2}\left(\cos(k_x\Delta x)-1\right)\left(\cos\left(\frac{\pi\Delta y}{Y_1}\right)-1\right)\Big] \\ & \times\Big[1+\frac{1}{6}\left(\cos(k_x\Delta x)-1\right)+\frac{1}{6}\left(\cos\left(\frac{\pi\Delta y}{Y_1}\right)-1\right)\Big]^{-1}. \end{aligned} \tag{48}$$

This is the dispersion relation modified due to the spatial discretization. Adding now the correction due to the Crank-Nicolson time discretization yields the dispersion relation

$$E(k_x) \;=\; \frac{\hbar}{i\Delta t}\ln\left(\frac{2i\hbar-\Delta t E_{\mathrm{space}}(k_x)}{2i\hbar+\Delta t E_{\mathrm{space}}(k_x)}\right) \tag{49}$$

for the discrete Schrödinger equation (analogous to (11)) with a time-harmonic plane wave solution. For a detailed analysis of the discrete dispersion relation we refer to [32, 33].

For the following simulation we solve the Schrödinger equation (1) by the difference equation (11) without external potential, i.e. $V = 0$. For realistic simulations of MOSFET–channels, (1) should be coupled to the self–consistent Coulomb potential inside the channel. Since we focus on DTBCs, we shall not include this here. But a coupling to the Poisson equation *inside* the computational domain does *not* change the derivation or discretization of our open BC (cf. [32]).

Fig. 7 shows the temporal evolution of the solution $|\psi(x, y, t)|$. In this simulation the stub length is first fixed to $L_1 = 32$nm. After 1.68ps the solution reaches (essentially) a steady state (*off-state* of the waveguide). Phenomenologically speaking, in this case only $1\frac{1}{2}$ wave packets "fit" into the stub (cf. Fig. 7(c)). Hence, they block the current flow through the waveguide. Then, at $t = 1.68$ps the stub is enlarged at once to $L_2 = 40.5$nm. After some transient phase, the solution converges to a new steady state (*on-state* of the waveguide, cf. Fig. 7(f)). Here, two wave packets "fit" into the stub, and the current can flow almost unblocked through the device.

Conclusion

In this chapter we have reviewed *discrete transparent boundary conditions* for the transient two dimensional Schrödinger equation. In particular, we discussed them for a fourth order *Numerov finite difference scheme*. Their numerical efficiency is demonstrated in numerical tests on a rectangular geometry as well as for quantum waveguide simulations (for details cf. [8, 10, 33]).

Acknowledgements

The first author (A.A.) was partly supported by the DFG–project AR 277/3–3 and the Wissenschaftskolleg *Differentialgleichungen* of the FWF.

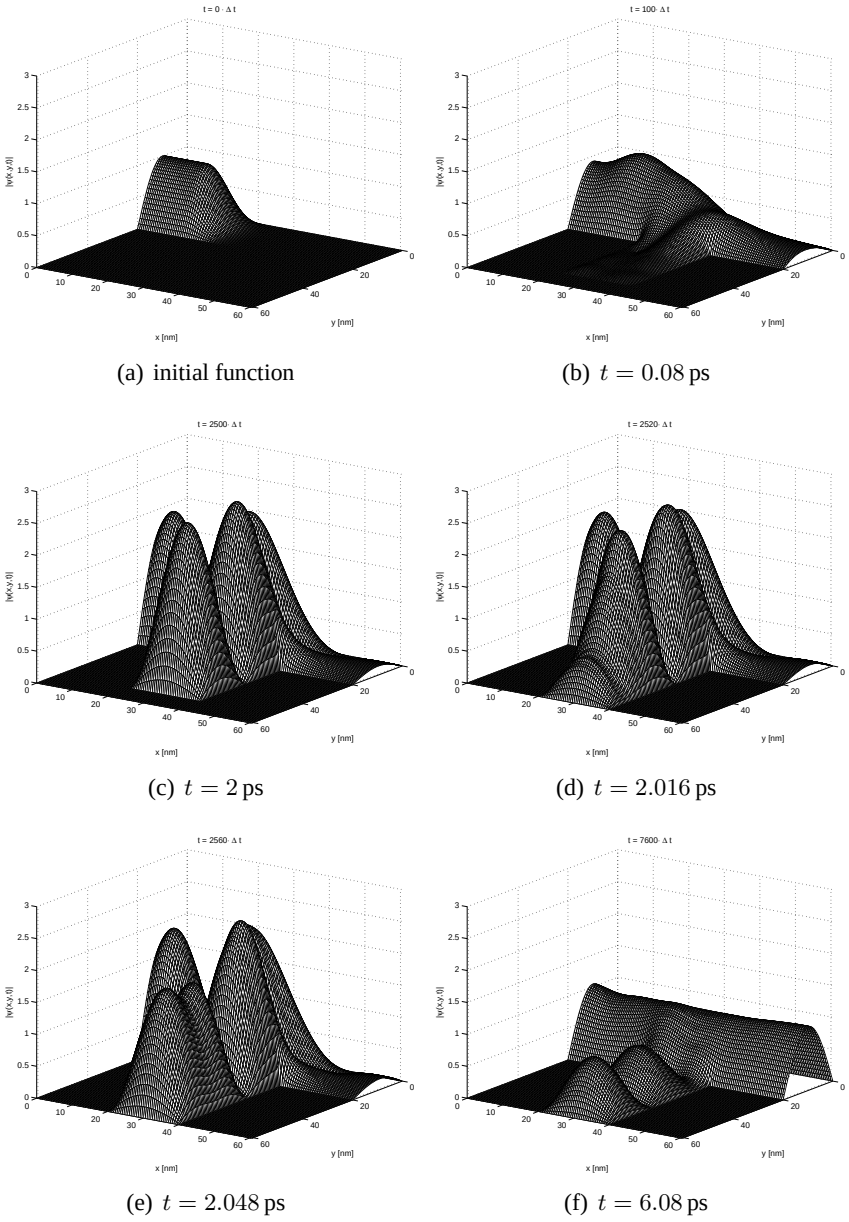

(a) initial function (b) $t = 0.08$ ps

(c) $t = 2$ ps (d) $t = 2.016$ ps

(e) $t = 2.048$ ps (f) $t = 6.08$ ps

Figure 7: Absolute value of the solution $\psi(x, y, t)$ of the time-dependent Schrödinger equation (46) on the T–shaped structure from Figure 2. The discretization parameters are $\Delta x = \Delta y = 0.25$nm, $\Delta t = 0.8$fs, $V = -E = -29.9$meV, $m_* = 0.067 m_0$. (c) shows the steady state corresponding to the short stub with $L_1 = 32$nm. (f) is the steady state for the long stub with $L = 40.5$nm.

References

[1] K. Aihara, M. Yamamoto and T. Mizutani, *Three–terminal conductance modulation of a quantum interference device using a quantum wire with a stub structure*, Appl. Phys. Lett. **63** (1993), 3595–3597.

[2] G. Allaire, A. Arnold, P. Degond, T.Y. Hou, *Quantum Transport — Modelling, Analysis and Asymptotics*, Lecture Notes in Mathematics 1946, Springer, Berlin (2008).

[3] B. Alpert, L. Greengard and T. Hagstrom, *Rapid evaluation of nonreflecting boundary kernels for time–domain wave propagation*, SIAM J. Numer. Anal. **37** (2000), 1138–1164.

[4] X. Antoine, A. Arnold, C. Besse, M. Ehrhardt and A. Schädle, *A Review of Transparent and Artificial Boundary Conditions Techniques for Linear and Nonlinear Schrödinger Equations*, Commun. Comput. Phys. **4** (2008), 729–796. (open–access article)

[5] J. Appenzeller, C. Schroer, T. Schäpers, A. v.d. Hart, A. Förster, B. Lengler and H. Lüth, *Electron interference in a T-shaped quantum transistor based on Schottky-gate technology*, Phys. Rev. B **53** (1996), 9959–9963.

[6] A. Arnold, *Numerically absorbing boundary conditions for quantum evolution equations*, VLSI Design **6** (1998), 313–319.

[7] A. Arnold, *Mathematical concepts of open quantum boundary conditions*, Transp. Theory Stat. Phys. **30** (2001), 561–584.

[8] A. Arnold, M. Ehrhardt and I. Sofronov, *Discrete transparent boundary conditions for the Schrödinger equation: Fast calculation, approximation, and stability*, Commun. Math. Sci. **1** (2003), 501–556.

[9] A. Arnold, M. Ehrhardt, M. Schulte and I. Sofronov, *Discrete transparent boundary conditions for the Schrödinger equation on circular domains*, submitted to: Commun. Math. Sci., 2008.

[10] A. Arnold and M. Schulte, *Transparent boundary conditions for quantum-waveguide simulations*, to appear in Mathematics and Computers in Simulation (2008).

[11] V.A. Baskakov and A.V. Popov, *Implementation of transparent boundaries for numerical solution of the Schrödinger equation*, Wave Motion **14** (1991), 123–128.

[12] N. Ben Abdallah, F. Méhats and O. Pinaud, *On an open transient Schrödinger-Poisson system*, Math. Models Methods Appl. Sci. **15** (2005), 667–688.

[13] L. Burgnies, *Mécanismes de conduction en régime ballistique dans les dispositifs électroniques quantiques*, Ph. D. thesis, Université des Sciences et Technologies de Lille, 1997.

[14] H.S. Carslaw and J.C. Jaeger, *Conduction of heat in solids*, Clarendon Press, Oxford, UK, 1959.

[15] A. Dedner, D. Kröner, I. Sofronov and M. Wesenberg, *Transparent Boundary Conditions for MHD Simulations in Stratified Atmospheres*, J. Comput. Phys. **171** (2001), 448–478.

[16] M. Ehrhardt, *Discrete Artificial Boundary Conditions*, Ph.D. Thesis, Technische Universität Berlin, 2001.

[17] M. Ehrhardt and A. Arnold, *Discrete Transparent Boundary Conditions for the Schrödinger Equation*, Riv. Mat. Univ. Parma **6** (2001), 57–108.

[18] M. Ehrhardt and R.E. Mickens, *Solutions to the discrete Airy equation: Application to parabolic equation calculations*, J. Comput. Appl. Math. **172** (2004), 183–206.

[19] M. Ehrhardt and A. Zisowsky, *Fast calculation of energy and mass preserving solutions of Schrödinger–Poisson systems on unbounded domains*, J. Comput. Appl. Math. **187** (2006), 1–28.

[20] M. Ehrhardt and A. Zisowsky, *Discrete non–local boundary conditions for Split–Step Padé approximations of the one–way Helmholtz equation*, J. Comput. Appl. Math. **200** (2007), 471–490.

[21] M. Ehrhardt, *Discrete transparent boundary conditions for Schrödinger–type equations for non–compactly supported initial data*, Appl. Numer. Math. **58** (2008), 660–673.

[22] M. Ehrhardt and C. Zheng, *Exact artificial boundary conditions for problems with periodic structures*, J. Comput. Phys. **227** (2008), 6877–6894.

[23] D.K. Ferry and S.M. Goodnick: *Transport in Nanostructures*, Cambridge University Press, Cambridge (1997).

[24] W.R. Frensley *Boundary conditions for open quantum systems driven far from equilibrium*, Rev. Mod. Phys. **62** (1990), 745–791.

[25] L. Greengard and J. Strain, *A fast algorithm for the evaluation of heat potentials*, Comm. Pure Appl. Math. **43** (1990), 949–963.

[26] T. Hagstrom, *Radiation boundary conditions for the numerical simulation of waves*, Acta Numerica **8** (1999), 47–106.

[27] G. Jing and M. S. Lundstrom, *A computational study of thin–body, double–gate, Schottky barrier MOSFETs*, IEEE Tran. on Elec. Dev. **49** (2002), 1897–1902.

[28] B. Mayfield, *Non-local boundary conditions for the Schrödinger equation*, Ph. D. thesis, University Rhode Island, Providence, RI (1989).

[29] C.A. Moyer, *Numerov extension of transparent boundary conditions for the Schrödinger equation in one dimension*, Amer. J. Phys. **72** (2004), 351–358.

[30] C.A. Moyer, *Numerical solution of the stationary state Schrödinger equation using discrete transparent boundary conditions*, Computing in Science and Engineering **8** (2006), 32–40.

[31] J.S. Papadakis, *Impedance formulation of the bottom boundary condition for the parabolic equation model in underwater acoustics*, NORDA Parabolic Equation Workshop, NORDA Tech. Note **143** (1982).

[32] M. Schulte, *Numerical Solution of the Schrödinger Equation on Unbounded Domains*, Ph.D. Thesis, Universität Münster, 2007.

[33] M. Schulte and A. Arnold, *Discrete transparent boundary conditions for the Schrödinger equation – a higher compact order scheme*, Kinetic and Related Models **1** (2008), 101–125.

[34] I.L. Sofronov, *Conditions for Complete Transparency on the Sphere for the Three–Dimensional Wave Equation*, Russian Acad. Sci. Dokl. Math. **46** (1993), 397–401.

[35] I.L. Sofronov, *Artificial Boundary Conditions of Absolute Transparency for Two- and Threedimensional External Time–Dependent Scattering Problems*, Euro. J. Appl. Math. **9** (1998), 561–588.

[36] I.L. Sofronov, *Non–reflecting inflow and outflow in wind tunnel for transonic time–accurate simulation*, J. Math. Anal. Appl. **221** (1998), 92–115.

[37] J. Wang, E. Polizzi and M. Lundstrom, *A three-dimensional quantum simulation of silicon nanowire transistors with the effective–mass approximation*, J. Appl. Phys. **96** (2004), 2192–2203.